Acta Oceanol. Sin., 2023, Vol. 42, No. 5, P. 25–34
https://doi.org/10.1007/s13131-022-2074-5
http://www.aosocean.com
E-mail: ocean2@hyxb.org.cn

Characteristics and mechanisms of the intraseasonal variability of sea surface salinity in the southeastern Arabian Sea during 2015–2020

Hui Teng[1], Yun Qiu[1, 2, 3, 4*], Xinyu Lin[1, 4], Xiwu Zhou[1, 4]

[1] Third Institute of Oceanography, Ministry of Natural Resources, Xiamen 361005, China

[2] Laboratory for Regional Oceanography and Numerical Modeling, Laoshan Laboratory, Qingdao 266237, China

[3] Southern Marine Science and Engineering Guangdong Laboratory (Zhuhai), Zhuhai 519082, China

[4] Fujian Provincial Key Laboratory of Marine Physical and Geological Processes, Xiamen 361005, China

Received 5 April 2022; accepted 16 May 2022

Abstract

Based on Soil Moisture Active Passive sea surface salinity (SSS) data from April 2015 to August 2020, combined with Objectively Analyzed Air-Sea Heat Flux and other observational data and Hybrid Coordinate Ocean Model (HYCOM) data, this work explores the characteristics and mechanisms of the intraseasonal variability of SSS in the southeastern Arabian Sea (SEAS). The results show that the intraseasonal variability of SSS in the SEAS is very significant, especially the strongest intraseasonal signal in SSS, which is located along the northeast monsoon current (NMC) path south of the Indian Peninsula. There are remarkable seasonal differences in intraseasonal SSS variability, which is very weak in spring and summer and much stronger in autumn and winter. This strong intraseasonal variability in autumn and winter is closely related to the Madden-Julian Oscillation (MJO) event during this period. The northeast wind anomaly in the Bay of Bengal (BOB) associated with the active MJO phase strengthens the East India Coastal Current and NMC and consequently induces more BOB low-salinity water to enter the SEAS, causing strong SSS fluctuations. In addition, MJO-related precipitation further amplifies the intraseasonal variability of SSS in SEAS. Based on budget analysis of the mixed layer salinity using HYCOM data, it is shown that horizontal salinity advection (especially zonal advection) dominates the intraseasonal variability of mixed layer salinity and that surface freshwater flux has a secondary role.

Key words: southeastern Arabian Sea, sea surface salinity, intraseasonal variability, air-sea interaction

Citation: Teng Hui, Qiu Yun, Lin Xinyu, Zhou Xiwu. 2023. Characteristics and mechanisms of the intraseasonal variability of sea surface salinity in the southeastern Arabian Sea during 2015–2020. Acta Oceanologica Sinica, 42(5): 25–34, doi: 10.1007/s13131-022-2074-5

1 Introduction

The southeastern Arabian Sea (SEAS) (0°–13°N, 65°–80°E; Fig. 1a) is dominated by the Indian monsoon, and the northeast monsoon prevails from November to March of the next year, while the southwest monsoon prevails from May to September (Schott et al., 2009). Driven by this monsoon, the upper circulation in this area reverses semiannually. The eastward southwest monsoon current occurs north of the equator in summer and reverses into a westward northeast monsoon current (NMC) in winter (Fig. 1a), providing a key dynamic passage for the water exchange between the Arabian Sea (AS) and the Bay of Bengal (BOB) (Narvekar et al., 2017).

Although located in the same latitude range in the North Indian Ocean, due to different atmospheric forcings, such as evaporation and precipitation, as well as land runoff, the upper salinity of the AS and BOB are significantly different and are the highest and lowest, respectively, in the Indian Ocean (Behara et al., 2019). The vast difference in salinity between these two basins enables the salinity exchange associated with the aforementioned monsoon circulation to play an important role in maintaining the salinity balance between the BOB and the AS (Zhang and Du, 2012) and consequently to have an important impact on the regional climate. During the northeast monsoon, the low-salinity waters from the BOB are transported by the East Indian Coastal Current (EICC) and the NMC into the SEAS to induce a barrier layer, which is the main cause of the formation and maintenance of the AS mini warm pool in spring (Nyadjro et al., 2012; Shankar and Shetye, 1997). This mini warm pool has an important role in modulating the onset date and intensity of the local monsoon (Vinayachandran et al., 2007). Thus, the study of salinity variations in the SEAS may contribute to our understanding of regional climate variability and prediction.

Several studies have been carried out to explore the variations in salinity and their mechanisms in SEAS. Prakash et al. (2012) analyzed the relationship between surface freshwater flux and sea surface salinity (SSS) in the northern Indian Ocean and indicated a highly positive linear correlation (R=0.74) between them in the AS. These authors pointed out that the variations in

Foundation item: The National Natural Science Foundation of China under contract No. 42130406; the Scientific Research Foundation of Third Institute of Oceanography, Ministry of Natural Resources under contract Nos 2022027 and 2018030; the Asian Countries Maritime Cooperation Fund under contract No. 99950410; the Global Change and Air-Sea Interaction Ⅱ under contract No. GASI-04-WLHY-01.

*Corresponding author, E-mail: qiuyun@tio.org.cn

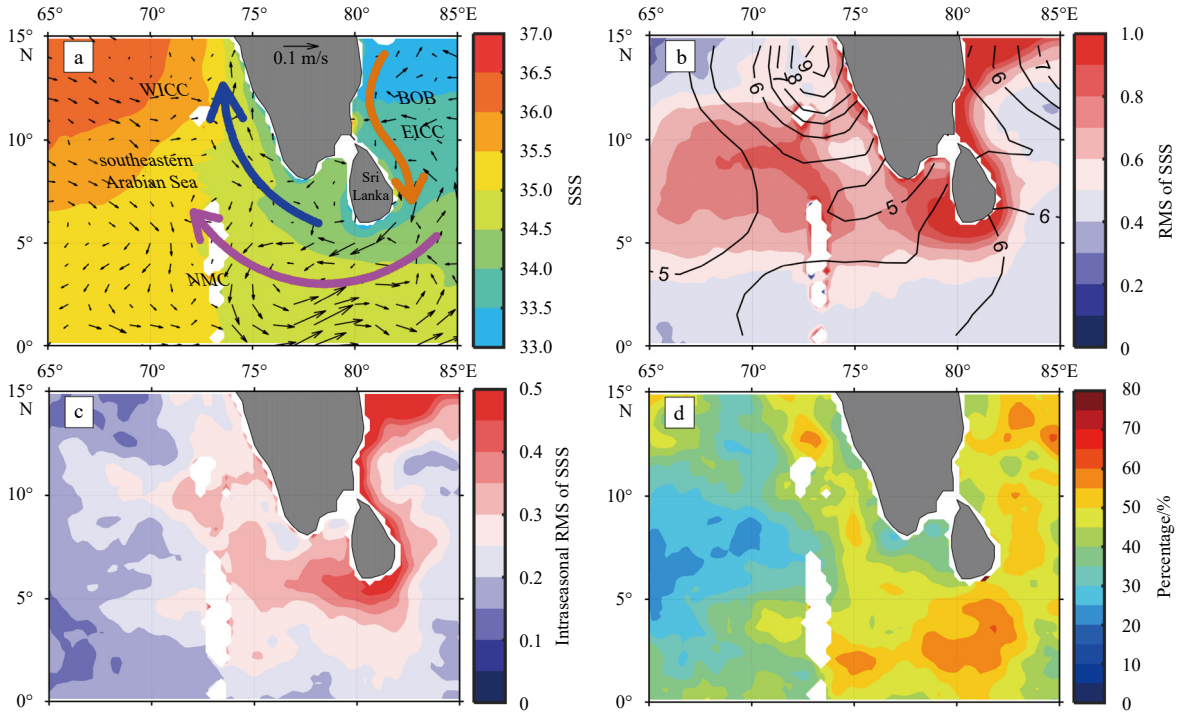

Fig. 1. Annual mean Soil Moisture Active Passive (SMAP) sea surface salinity (SSS) and Ocean Surface Current Analysis Real-time surface currents (arrows; unit: m/s) (a), root mean square (RMS) of SMAP SSS and RMS of evaporation minus precipitation (*E*–*P*, contours; unit: mm/d) (b), intraseasonal RMS of SMAP SSS (c), and percentage of intraseasonal RMS to total RMS for SSS (d). The purple line represents the pathway of the northeast monsoon current (NMC) around Sri Lanka, and the orange line represents the pathway of the East India Coastal Current (EICC), and the blue line represents the pathway of the West India Coastal Current (WICC). BOB: Bay of Bengal.

SSS in the AS are dominated by the surface freshwater flux. Rao and Sivakumar (2003) showed remarkable seasonal variabilities in SSS in the northern coastal regions along the BOB, northwestern AS and SEAS, and ocean advection was suggested to make an important contribution to the seasonal variation in SSS in these two parts of the AS. Zhang and Du (2012) further confirmed the conclusion of Rao and Sivakumar (2003). The authors showed that the surface freshwater flux cannot explain the seasonal variability in SSS in the SEAS. Instead, oceanic advection is the main reason for the decrease in SSS in winter and increase in SSS in summer. In winter, the NMC carries fresher water from the BOB westward into the SEAS, resulting in a decrease in SSS. In contrast, in summer, the southwest monsoon current transports high-salinity water from the northwestern AS, increasing the SSS in the SEAS. In the central part of the southern AS and the equatorial Indian Ocean, oceanic advection also dominates the seasonal variability in SSS (Da-Allada et al., 2015).

In addition to the abovementioned seasonal variability, a recent study (Jayarathna et al., 2018) has shown that ocean advection is also the main cause of the interannual variability in SSS in the central and northern AS and the equatorial Indian Ocean. Wu et al. (2020) analyzed the influence of El Niño events on SSS over the central equatorial Indian Ocean, and found that the wind-driven anomalous zonal advection plays an important role in SSS variability during the El Niño events associated with the forcing from the anomalous Walker Circulation over the equatorial Indian Ocean. In the southeastern Indian Ocean, ocean salinity in upper 200 m presents notable decadal variability and it is dominantly resulted from the anomalous meridional advection related to a zonal dipole pattern of sea level anomaly, forced by the tropical Pacific decadal variability via interbasin teleconnection (Wu et al., 2021). In contrast, due to the lack of high-quality observational data, the understanding of the intraseasonal variation in SSS in the tropical Indo-Pacific Ocean, including our study region, is insufficient. A recent study (Matthews et al., 2010) suggested that precipitation in the tropical Indo-Pacific Ocean shows sharp intraseasonal variability and consequently hypothesized that it may dominate the changes in SSS. However, based on the Ocean General Circulation Model, Schiller and Godfrey (2003) suggested that the roles of oceanic advection on the intraseasonal variability in SSS are comparable to those of surface freshwater forcing in the tropical Indian Ocean. Li et al. (2015) investigated intraseasonal SSS variability associated with Madden-Julian Oscillation (MJO) events using satellite observations and numerical models and discovered that in areas of the BOB and the equatorial eastern Indian Ocean with salinity fronts, the strong cross-frontal salinity advection induced by ocean circulation dominates intraseasonal salinity variability. The roles of precipitation and evaporation are secondary. The diverse mechanisms of intraseasonal SSS variability revealed by the aforementioned studies reflect that the impacts of atmospheric and oceanic forcings on SSS variability are very complicated and have a regional dependence.

As the SEAS frequently suffers from MJO activities (Wang et al., 2012), SSS may certainly have intraseasonal variation (Li et al., 2015). However, presently, the understanding of intraseasonal SSS variation in the SEAS is still ambiguous. MJO events have a significant phase locking, which is more active in winter (Li et al., 2020). Under the merged influences from atmospheric forcings and ocean dynamic processes associated with MJO, what are the seasonal characteristics of the intraseasonal SSS

variability in the SEAS? Which processes induce such an intraseasonal variation? This is the key scientific question to be explored in this study. The remainder of the paper is organized as follows: Section 2 introduces the data and methods; Section 3 analyzes the temporal and spatial distribution characteristics of intraseasonal SSS variability; the related mechanism is discussed in Section 4 and Section 5 presents the conclusions.

2 Data and methods

2.1 *Data*

The daily Soil Moisture Active Passive (SMAP) JPL v4.3 SSS data with a spatial resolution of 0.25°×0.25° during April 4, 2015, and August 22, 2020, are provided by the Asia-Pacific Data-Research Center (APDRC). The daily salinity data are utilized to analyze the characteristics of SSS variation.

The daily Global Precipitation Climatology Project (GPCP) (Huffman et al., 1997) precipitation data, with a spatial resolution of 1°×1°, are provided by the APDRC. The GPCP precipitation integrates the surface rain gauge of the Global Precipitation Climatology Center and satellite-based observations, which can well reflect the temporal and spatial patterns of rainfall in the tropical oceans (Xu and Gao, 2018). The daily Objectively Analyzed Air-Sea Heat Flux evaporation data with a spatial resolution of 1°×1° are provided by the Woods Hole Oceanographic Institution. Ocean Surface Current Analysis Real-time (OSCAR) surface current data are provided by the APDRC. The data have a temporal resolution of 5 d and a spatial resolution of (1/3)°×(1/3)°. The daily Advanced Scatterometer (ASCAT) sea surface wind data, with a spatial resolution of 1°×1°, are released from the APDRC. The daily 2.5°×2.5° outgoing longwave radiation (OLR) data are obtained from the National Oceanic and Atmospheric Administration (NOAA). All the aforementioned observational data have a time span from April 4, 2015 to August 22, 2020, which is equivalent to that of SMAP SSS. These data are employed to explore the dynamics of SSS intraseasonal variability.

The daily output of the Hybrid Coordinate Ocean Model (HYCOM) version 3.0, including temperature, salinity, current, and surface freshwater flux available for the period of April 4, 2015 to November 27, 2018, is downloaded from the HYCOM website (https://www.hycom.org/). The HYCOM data have a spatial resolution of (1/12)°×(1/12)° in the horizontal direction and have 10 layers above 200 m with the depths of each layer being 0 m, 10 m, 20 m, 30 m, 50 m, 75 m, 100 m, 125 m, 150 m, 200 m. HYCOM data are used to calculate the salinity budget in the mixed layer.

Since this study focuses on the intraseasonal variability of salinity, all the data mentioned above are band-passed with a 30–90 d filter to extract the desired signal of intraseasonal oscillations (hereafter referred as anomalies in the captions of the figures) before the analysis. According to a previous study (Wang et al., 2016), the months of spring, summer, autumn and winter are defined as March–May, June–August, September–November, and December–February of the following year, respectively.

2.2 *Methods*

Following Feng et al. (1998), the salinity conservation equation for the mixed layer can be expressed as

$$\frac{\partial S}{\partial t}=-\frac{S_0(P-E)}{h}-\left(u\frac{\partial S}{\partial x}+v\frac{\partial S}{\partial y}\right)-w_{\mathrm{e}}\frac{S-S_{-h}}{h}, \tag{1}$$

the terms in Eq. (1) from left to right are the salinity tendency, sea surface freshwater flux, horizontal advection, and vertical entrainment. S is the mixed-layer salinity; u and v are the zonal component and meridional component, respectively, of mixed-layer velocity; S_0 is SSS; S_{-h} is the salinity just below the mixed layer; P and E are the precipitation rate and evaporation rate, respectively; w_{e} is the vertical entrainment velocity, $w_{\mathrm{e}}=\frac{\mathrm{d}h}{\mathrm{d}t}+w|_{-h}$, where $w|_{-h}=h\left(\frac{\partial u}{\partial x}+\frac{\partial v}{\partial y}\right)$ is the vertical entrainment velocity just below the mixed layer; and h is the depth of the mixed layer, which is defined as the depth when the density $\sigma_\theta=\sigma_{(z=10)}+\sigma_\Delta$, where $\sigma_{(z=10)}$ is the density of 10 m layer, and σ_Δ is the density increase caused by the temperature drop of 0.2℃ when the salinity of 10 m layer remains unchanged (Kara et al., 2000; Price et al., 1986).

To separate the intraseasonal cycle, each variable is divided into two parts: the climatological mean cycle and intraseasonal variability (e.g., $S=\bar{S}+S'$). By disregarding the higher-order nonlinear terms, Eq. (1) can be rewritten as

$$\frac{\partial S'}{\partial t}=-\frac{\bar{S}_0(P-E)'}{h}-\left(\bar{u}\frac{\partial S'}{\partial x}+u'\frac{\partial \bar{S}}{\partial x}+\bar{v}\frac{\partial S'}{\partial y}+v'\frac{\partial \bar{S}}{\partial y}\right)-w'_{\mathrm{e}}\frac{\overline{(S-S_{-h})}}{h}. \tag{2}$$

As the entrainment term is relatively small compared with the horizontal advection term and the sea surface freshwater flux (Rao and Sivakumar, 2003; Da-Allada et al., 2015), it is ignored in this study.

3 Characteristics of intraseasonal variability of SSS in the SEAS

Figure 1a shows the spatial distribution of the annual mean SSS in the SEAS. The SSS value is high in the northwest and low in the southeast, with a difference of ~3 in salinity. The lowest salinity (33.5) appears in the coastal regions along the southern tip of the Indian Peninsula. The low-salinity water originates from the BOB, which is transported into the SEAS by the EICC, NMC and West Indian Coast Current (Gopalakrishna et al., 2005). The movement of the BOB low-salinity water in the SEAS is also revealed in the annual mean surface current (Fig. 1a). A strong westward current originating from the BOB extends along the southern coast of Sri Lanka into the SEAS to approximately 74°E and is divided into two branches. The first branch flows southward and the remaining branch flows northwestward along the western coast of the Indian Peninsula. In the junction area of low- and high-salinity water between 3°N and 10°N, there is a very strong gradient of salinity aligning mostly in the zonal direction, particularly in the coastal regions from the Indian Peninsula to southern Sri Lanka (Fig. 1a). Correspondingly, in these regions with a strong salinity gradient, the SSS root mean square (RMS) is much larger (>0.6), which does not match the locations with a large RMS of evaporation minus precipitation (E–P, Fig. 1b). We note that the large RMS of E–P (>6 mm/d) is located west of the Indian Peninsula between 10°N and 15°N, with a maximum of 9 mm/d. This mismatch in the RMS of SSS and E–P suggests that oceanic advection may play an important role in the SSS variability in the study region (Zhang and Du, 2012).

The intraseasonal variation in SSS (Fig. 1c) is larger than 0.2 in most parts of the SEAS and accounts for 30%–60% of the total RMS (Fig. 1d), indicating that the intraseasonal signal is one of the major signals of SSS variability in the study region. The strong intraseasonal variation in SSS (>0.3) is located at the western boundary of the BOB and along the coast of Sri Lanka, extending

westward along the path of the NMC into the SEAS until approximately 73.5°E. Figure 2 shows the seasonal distribution for the intraseasonal RMS of SSS. The intraseasonal variability of SSS in spring and summer is very weak in most parts of the SEAS (Figs 2a, b). In contrast, the intraseasonal variability in SSS is much stronger in autumn and winter (Figs 2c, d). During these two seasons, the strong intraseasonal variability with RMS values larger than 0.35 is observed in almost the same regions as the aforementioned total intraseasonal variability (Fig. 1c) and peaks in the coverage in winter (Fig. 2d).

As variations in SSS may be caused by surface freshwater flux and oceanic advection (Sun et al., 2019), the distribution of *E*–*P* and the zonal component of surface current (Fig. 3) reveal their possible impact on the intraseasonal variability in SSS. Unlike SSS, the seasonal variation in intraseasonal *E*–*P* RMS is weak in most parts of the SEAS, and *E*–*P* RMS in spring and summer is comparable with that in autumn and winter (Fig. 3). However, the intraseasonal zonal currents show a seasonality similar to that of SSS. In autumn and winter, the strong intraseasonal variability of the zonal current is present in the western boundary of the BOB, the coast of Sri Lanka, and along the path of the NMC south to the Indian Peninsula, the regions where the strong intraseasonal SSS RMS is located (Figs 3c, d), and is much stronger than that in spring and summer (Figs 3a, b). Unlike zonal current and SSS, the distribution of intraseasonal meridional currents indicates a very weak seasonal variation (figure is not shown). The high consistency between zonal current and SSS suggests that oceanic advection (i.e., zonal current) may have a more important role in the intraseasonal variability of SSS compared with *E*–*P*.

4 Mechanisms of intraseasonal variability of SSS

4.1 *Composite analysis using observation data*

The previous analysis reveals that the intraseasonal variability in SSS in the SEAS is associated with surface freshwater flux and oceanic advection. To further illustrate their roles in the SSS variations, Fig. 4 shows the daily SSS, *E*–*P* and zonal current in region A. Region A is located in the path of the NMC to the south of the Indian Peninsula (Fig. 3d), where the intraseasonal variability in SSS, *E*–*P* and surface zonal current is very significant in autumn and winter (Figs 3c, d). The intraseasonal variability characteristics of SSS presented in the time series are consistent with Fig. 2. The intraseasonal variability in SSS is much stronger in autumn and winter than in spring and summer. During April 2015 and August 2020, there are four strong intraseasonal oscillation events, with the variation in SSS exceeding 1.5 times the standard deviation (Fig. 4). All of these events occur in autumn and winter. Correspondingly, both *E*–*P* and zonal currents indicate stronger variations, exceeding their 1.5 standard deviations during these events (Figs 4a, b). An increasing (decreasing) SSS is associated with a positive (negative) *E*–*P* anomaly and an eastward (westward) zonal current anomaly. The correlation is highest when the SSS leads *E*–*P* by 19 d and lags the zonal current by 3 d, with positive correlation coefficients of 0.45 and 0.70, respectively, which are significant at the 99% confidence level. These close correlations indicate that both the surface freshwater flux and the advection of surface currents contribute to the intraseasonal variability in SSS, and the latter has a greater impact based on the correlation coefficients.

To elucidate the dynamic linkage between oceanic advection and SSS, including the role of surface freshwater flux, we select

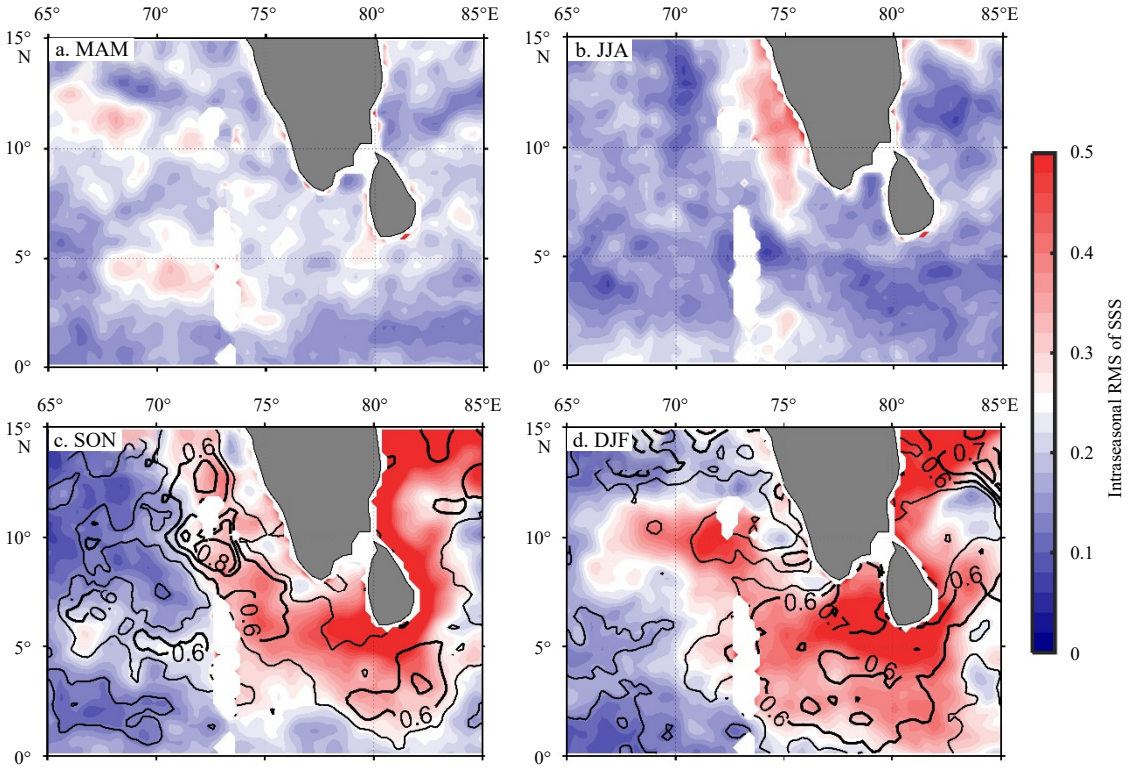

Fig. 2. Seasonal distribution for the intraseasonal root mean square (RMS) of SMAP sea surface salinity (SSS): spring (March–May, MAM) (a), summer (June–August, JJA) (b), autumn (September–November, SON) (c), and winter (December–February, DJF) (d). The contours in c and d represent the ratio of intraseasonal RMS to total RMS for SSS.

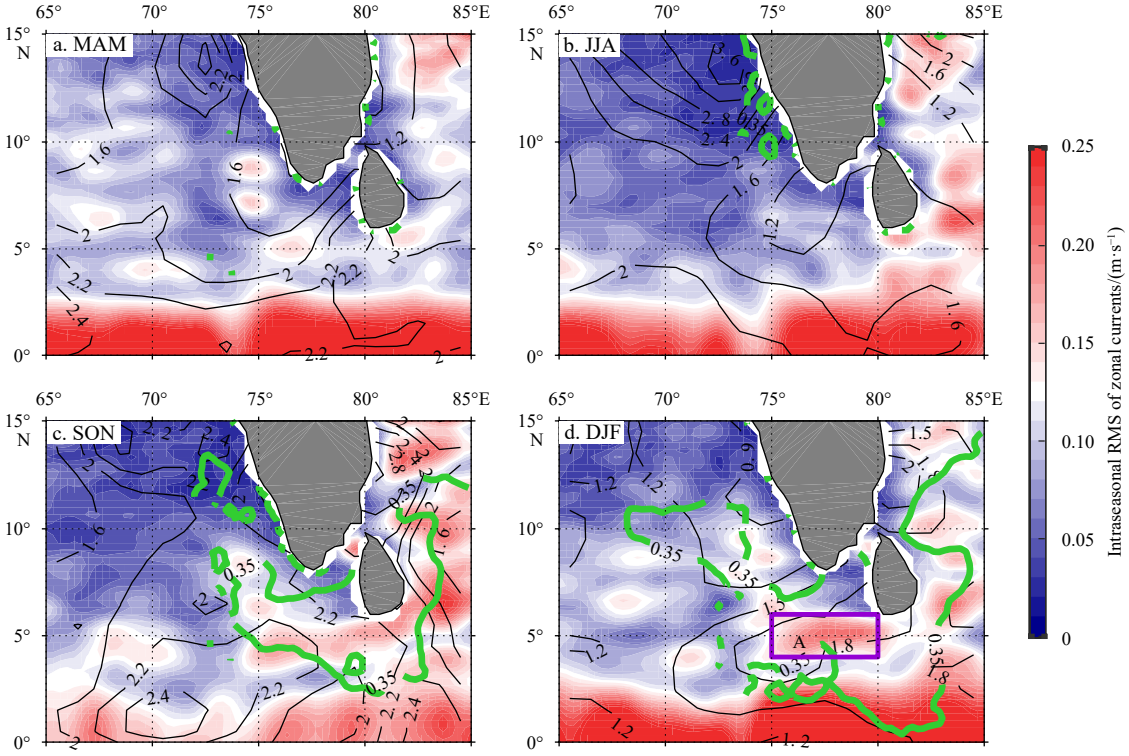

Fig. 3. Seasonal distribution of the intraseasonal root mean square (RMS) of OSCAR zonal currents and of *E*–*P* (contours; unit: mm/d): spring (a), summer (b), autumn (c), and winter (d). The areas bounded by thick green curves represent the regions with an intraseasonal SSS RMS larger than 0.35. Region A (4°–6°N, 75°–80°E) bounded by purple lines in d represents a region with strong intraseasonal variability in the southeastern Arabian Sea.

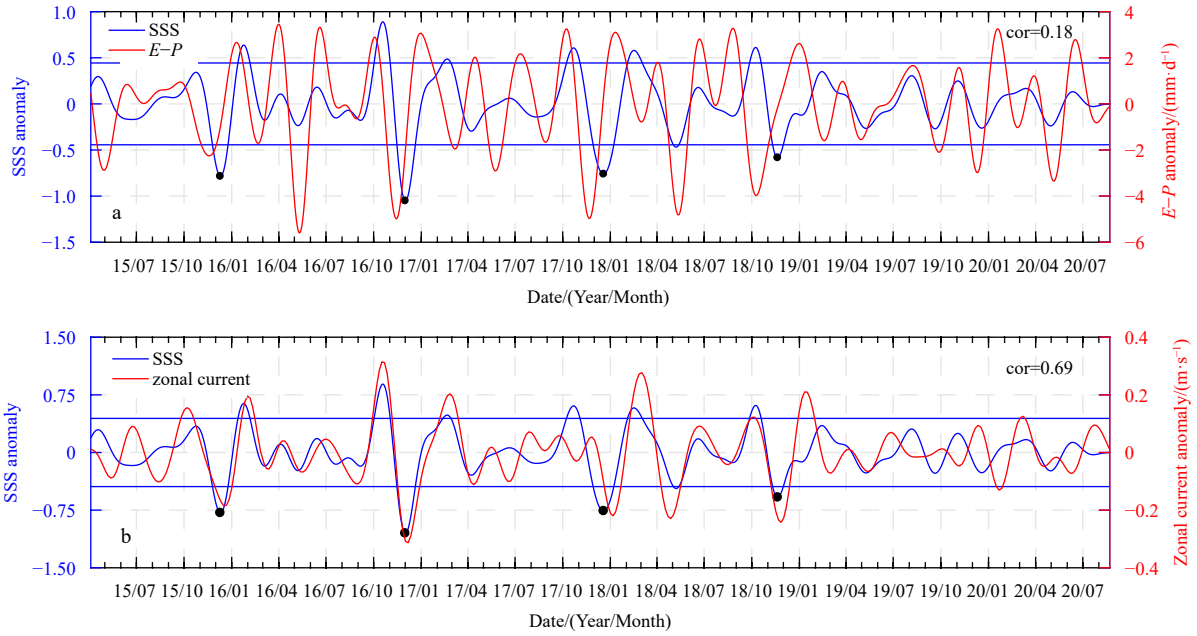

Fig. 4. Time series averaged in region A (shown in Fig. 3d) for: sea surface salinity (SSS) anomaly (blue curves) and *E*–*P* anomaly (red curves) (a), SSS anomaly and zonal current anomaly (b). The blue line is 1.5 times the standard deviation of the SSS anomaly. The dark points represent the lowest anomalous salinity for the strong intraseasonal SSS events. cor: correlation coefficient.

the abovementioned four strong intraseasonal events to examine the evolution process and driving mechanism of SSS (Figs 5, 6, and 7). Here, we select the date with the minimum salinity of each event as the reference time (0 d) and the composite from –40 d to +40 d at a 10-d interval.

The composites of atmospheric circulation clearly show the evolution of MJO events (Fig. 5). During the active MJO phase (–40–0 d), the southern AS and the western equatorial Indian Ocean are controlled by a cyclonic anomalous wind, and the northeasterly wind prevails over the BOB. The convection is

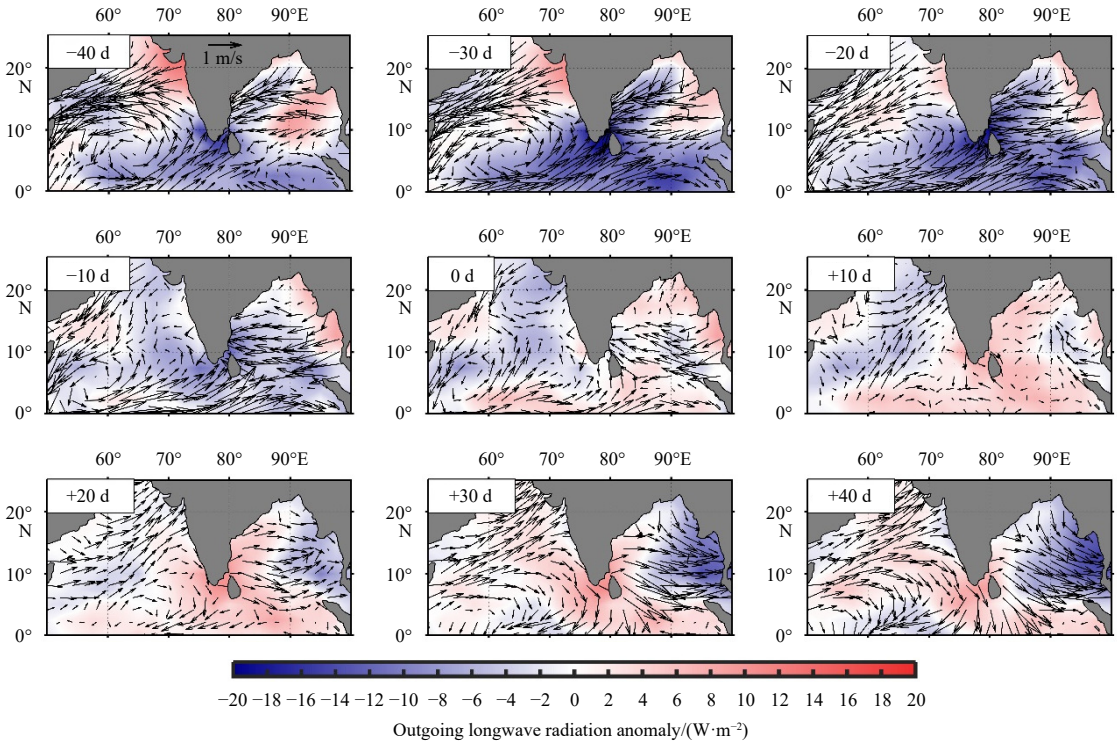

Fig. 5. Composite surface wind anomaly (arrows, unit: m/s) and outgoing longwave radiation anomaly from –40 d to +40 d with 10-d intervals for the four strong intraseasonal events listed in Fig. 4. The date with the minimum salinity of each event is selected as the reference time (0 d).

strengthened over most parts of the AS, BOB and equatorial Indian Ocean. The anomalous atmospheric circulation peaks during the period of –30–−20 d, with an anomalous strong convection center located around the SEAS. During the suppressed MJO phase (+10 –+40 d), the pattern of atmospheric circulation anomalies reverses and peaks at +30–+40 d. During this phase, the AS and the equatorial Indian Ocean are controlled by anomalous anticyclonic winds, and westerly winds prevail in the BOB.

Forced by the aforementioned MJO-related surface wind, the SSS in region A exhibits a very significant intraseasonal oscillation feature (Figs 6 and 7). On day –40, the anomalous eastward currents associated with the cyclonic wind anomalies (Fig. 5) transport Arabian salty water from west to east, increasing the salinity to a maximum of 1 in region A. Negative salinity anomalies begin to appear north of 10°N in the western boundary of the BOB and the equatorial eastern Indian Ocean. The formation of the anomalous low salinity is related to the MJO-induced precipitation enhancement (Fig. 7) and the southward transport of low salinity water (Fig. 6). From –30 d to 0 d, with a gradual weakening of cyclonic wind, the anomalous eastward flow weakens and retreats westward. Consequently, the anomalous high salinity in region A weakens and retreats westward. The anomalous low-salinity water extends southward along the western boundary of the BOB by the anomalous strong EICC and reaches the northeast coast of Sri Lanka at –30 d. Bypassing Sri Lanka Island, the low salinity anomalies are transported into the SEAS by the anomalous strong NMC, the impact from which the salinity of region A reaches the lowest at 0 d. The anomalous low salinity gradually weakens and continues to expand westward and northwestward by the anomalous currents and covers most parts of the SEAS at +40 d. From +20 d to +40 d, the anomalous low salinity east of 75°E gradually reverses to a positive anomaly because of the weakening and even reversal of the anomalous westward current.

The good consistency of the intraseasonal variability between SSS and the surface current indicates that oceanic advection has a dominant role in MJO-related SSS variations in the SEAS. During autumn and winter, MJO events induce the anomalous low-salinity water in the BOB to be transported to the SEAS, resulting in the strong intraseasonal variability of SSS.

In addition to oceanic advection, MJO-related rainfall may also contribute to the intraseasonal variability in SSS. During the active MJO phase (–40–0 d), the strongest convection center in the SEAS mentioned above (Fig. 5) increases the precipitation and consequently amplifies the anomalous low-salinity water in this region during the active MJO phase. Similarly, during the suppressed MJO phase (+10 –+40 d), the decrease in precipitation causes the weakening and reversal of the anomalous low-salinity water formation in the active MJO phase (Fig. 7).

4.2 *Analysis of the salinity budget in 2016 based on HYCOM output*

The HYCOM output is used to quantify the impact of oceanic advection and surface freshwater flux on the intraseasonal variability of SSS. Before analysis, the HYCOM data are verified with SMAP salinity (Fig. 8). The spatial pattern of SSS in the HYCOM during winter is consistent with that of SMAP (Fig. 8a), except in the coastal regions where HYCOM SSS is approximately 0.5 higher than SMAP SSS. Similarly, the distribution of the HYCOM SSS RMS and intraseasonal RMS (Figs 8b, c) are also well matched with that of SMAP SSS (Figs 1b, c) in the open ocean. Both datasets show that strong RMS and intraseasonal values are located between 5°N and 10°N and that their values are comparable. In contrast, the RMS and intraseasonal RMS of HYCOM SSS are much smaller than those of SMAP in the coastal regions from Sri Lanka Island to the west of the Indian Peninsula. This mismatch may be attributed to the deficiency of the HYCOM in detecting

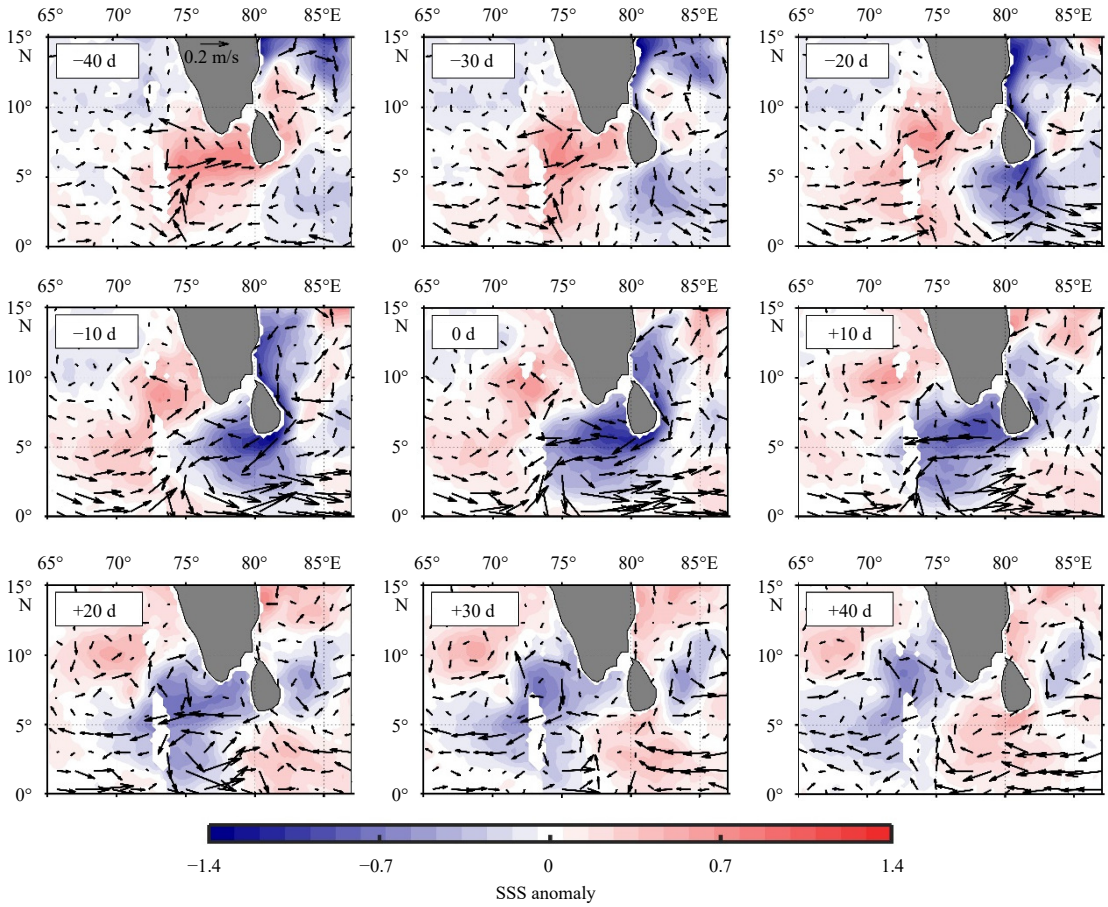

Fig. 6. Composite sea surface salinity (SSS) anomalies and surface current anomalies (arrows, unit: m/s) from –40 d to +40 d with 10-d intervals for the four strong intraseasonal events listed in Fig. 4. The date with the minimum salinity of each event is selected as the reference time (0 d).

the low salinity signals in the coastal regions, as noted in Fig. 8a.

Comparing the intraseasonal variability of HYCOM SSS with that of SMAP SSS in region A (Fig. 8d) reveals that in the overlapping period of these two datasets (i.e., April 2015–November 2018), the HYCOM has captured all three strong intraseasonal events shown in SMAP SSS during the winter of 2016–2018 (Fig. 4). Among the three intraseasonal events, the HYCOM has the best simulation of the 2016 winter event, and its phase and amplitude show agreement with those of SMAP. In contrast, in the remaining two winter events of 2017 and 2018, their amplitudes are significantly weaker than the SMAP observations, and their phases lag the observations by ~10–30 d. The evolution of the 2016 winter event by the HYCOM output (Fig. 9) is highly consistent with the SMAP observations (figure not shown). These good consistencies confirm the reliability of the HYCOM data, particularly for the 2016 winter event. Thus, the HYCOM output is selected to assess the relative importance of ocean dynamics in driving SSS variability during the 2016 winter event.

Selecting December 20, 2015, the date corresponding to the minimum salinity value of the 2016 event, as a reference point (0 d), the evolution of SSS can be divided into two stages (Fig. 8d): Stage 1 (–40–0 d) is the salinity decline stage that corresponds to the active MJO phase (Fig. 5), and Stage 2 (0 –+40 d) is the salinity increase stage (Fig. 8d) that corresponds to the suppressed MJO phase. The mixed-layer salinity budget of region A for these two stages is shown in Fig. 10. In Stage 1, the negative salinity tendency ($-0.026\ d^{-1}$) is mainly caused by the horizontal advection term ($-0.026\ d^{-1}$, Fig. 10a) and is mostly contributed by zonal advection ($-0.032\ d^{-1}$), and meridional advection ($0.006\ d^{-1}$) partially offsets the decreasing trend of mixed layer salinity (Fig. 10b). In addition, the freshwater flux ($-0.019\ d^{-1}$) also contributed significantly to the salinity tendency. In Stage 2, the mixed layer salinity tendency ($0.029\ d^{-1}$) is mainly contributed by the horizontal advection term ($0.036\ d^{-1}$), with a larger impact from zonal advection compared with meridional advection ($0.025\ d^{-1}$ vs. $0.011\ d^{-1}$). The contribution of freshwater flux is positive but relatively small ($0.012\ d^{-1}$). The residual term that represents small-scale processes decreases the signal of the salinity anomaly in both stages. Thus, the HYCOM results confirm the dominant role of oceanic advection in causing the intraseasonal variability of SSS in the SEAS during an MJO event.

5 Summary

In this study, SMAP SSS, Objectively Analyzed Air-Sea Heat Flux evaporation, GPCP precipitation, ASCAT wind, OLR data and the HYCOM model output are used to explore the characteristics and mechanism of intraseasonal variability of SSS in the SEAS for the period of April 2015 to August 2020.

The results reveal that the intraseasonal variability of SSS in the SEAS is remarkable. The strongest intraseasonal variability is located along the path of the NMC south of the Indian Peninsula. The intraseasonal variability in SSS also indicates obvious seasonality, which is weak in spring and summer and strong in autumn and winter. All four strong intraseasonal events from April

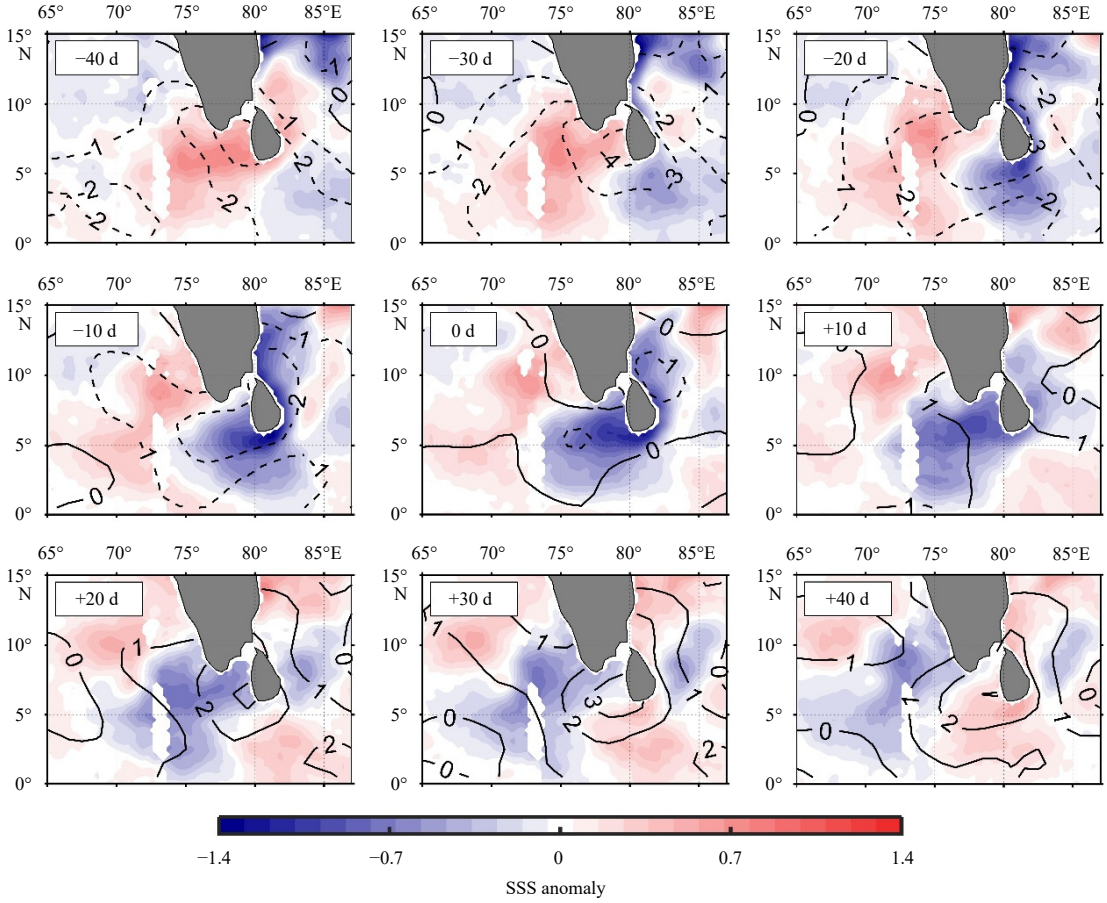

Fig. 7. Composite *E*–*P* anomalies (contours, unit: mm/d) from −40 d to +40 d with 10-d intervals for the four strong intraseasonal events listed in Fig. 4. The date with the minimum salinity of each event is selected as the reference time (0 d). Composite sea surface salinity (SSS) anomalies are also shown for comparison.

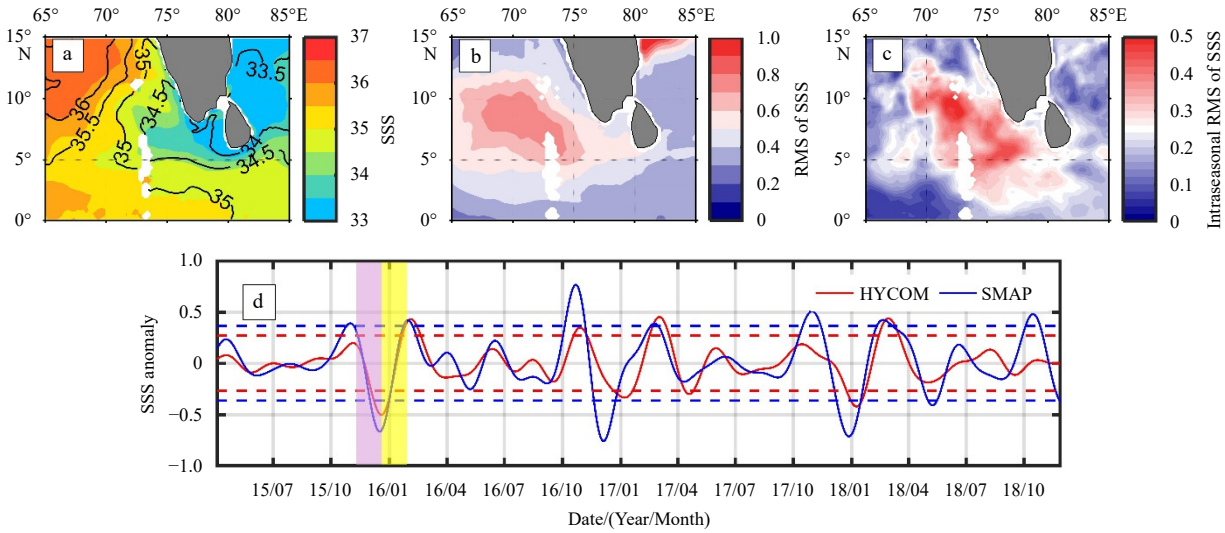

Fig. 8. Soil Moisture Active Passive (SMAP) SSS and Hybrid Coordinate Ocean Model (HYCOM) SSS (contours) for winter during 2015 and 2018 (a), RMS of HYCOM SSS (b), intraseasonal RMS of HYCOM SSS (c), and time series of the HYCOM SSS anomaly (blue curves) and SMAP SSS anomaly (red curves) of region A (d). The purple shading and yellow shading in d represents Stage 1 and Stage 2, respectively. The red (blue) dashed line represents 1.5 times the standard deviation of HYCOM (SMAP) SSS.

2015 to August 2020 occur in autumn and winter.

The composite analysis of these strong intraseasonal events shows that the strong intraseasonal variability of SSS in autumn and winter is mainly caused by MJO events. During the active MJO phase, MJO-related, cyclonic anomalous wind (Fig. 5) induces the anomalous eastward current to transport Arabian salty water from west to east, increasing SSS in the SEAS. The northeasterly/easterly anomalies in the BOB-associated MJO enhance

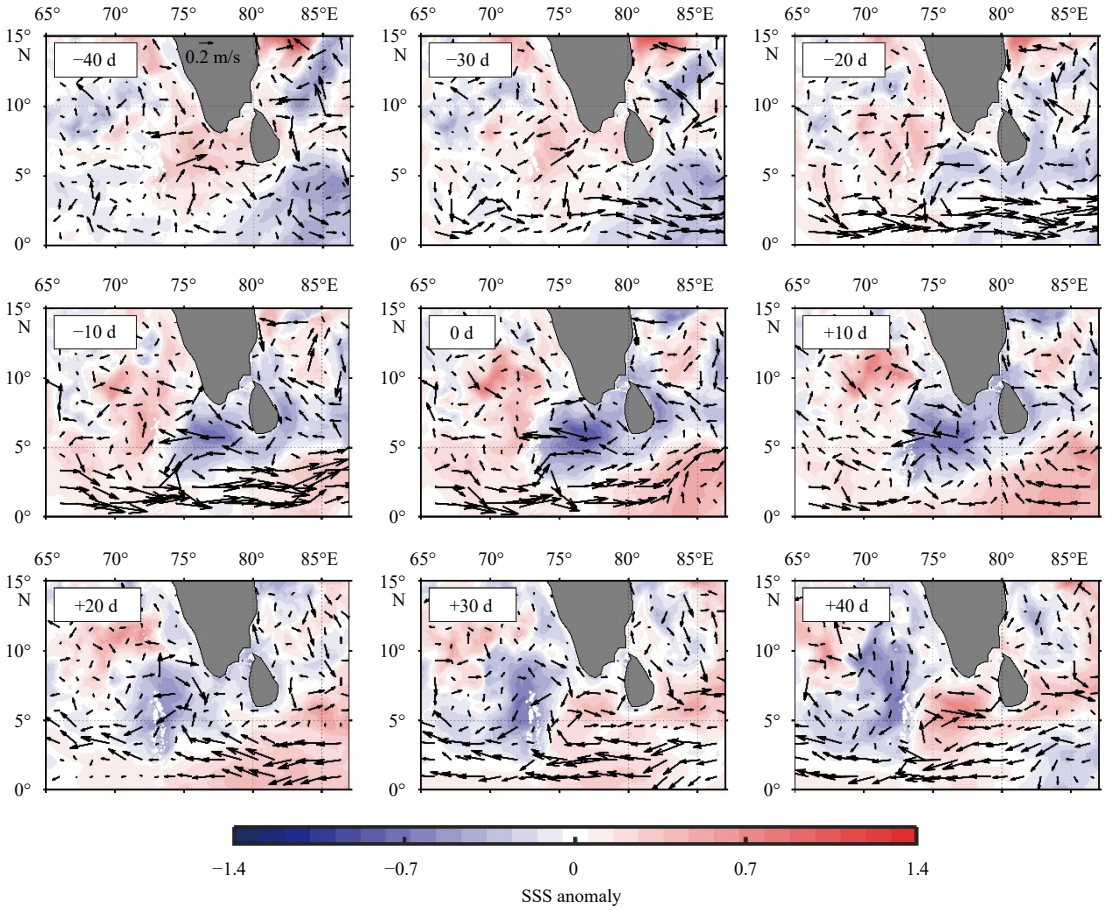

Fig. 9. Evolution process of the HYCOM SSS anomaly and surface current anomaly (arrows; unit: m/s) from –40 d to +40 d with 10-d intervals for the strong intraseasonal event in 2016 winter. The date with the minimum salinity of this event is selected as the reference time (0 d).

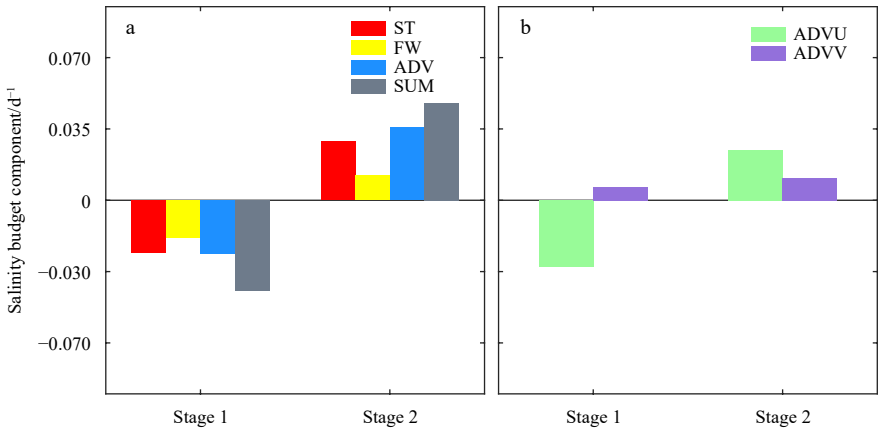

Fig. 10. Salinity budget components of the mixed layer salinity anomaly over region A for the strong intraseasonal event in 2016 winter calculated from the HYCOM output. In a, ST is the tendency of the mixed layer salinity anomaly; FW and ADV represent the tendencies of the mixed layer salinity anomaly caused by surface freshwater flux and horizontal advection, respectively; the sum of these two terms is denoted as SUM. ADVU and ADVV in b as shown in a but for zonal advection and meridional advection, respectively.

the EICC and NMC, causing more BOB freshwater to be transported to the SEAS. The BOB freshwater gradually overwhelms the salty anomaly into negative anomalous salinity in the SEAS, with the lowest anomalous salinity along the path of the NMC south to the Indian Peninsula. In addition, the strong precipitation in the active MJO phase also contributed to the decrease in salinity in the study area. During the suppressed MJO phase, the negative salinity anomalies gradually weaken and reverse to positive anomalies in the SEAS because of the variations in surface currents and the decreased precipitation.

The HYCOM data can well reproduce the evolution process of the strong intraseasonal oscillation events occurring in the winter

of 2016. A mixed-layer salinity budget analysis of the HYCOM output demonstrates that the contribution of the horizontal advection dominates the intraseasonal variability of SSS with much larger impacts from zonal advection compared with meridional advection. To a lesser degree, surface freshwater flux also contributes to the variability in SSS.

Although ocean salinity plays an important role in the upper-ocean stratification and regional climate in tropical Indian Ocean, the intraseasonal salinity variability in SEAS has not yet been well investigated. The present study finds that strong intraseasonal variability of SSS occurs in autumn and winter in the SEAS. The zonal advection associated with MJO events during autumn and winter plays a dominant role on the variability of salinity. Given that the intraseasonal variability of SSS can affect the salinity stratification in the upper ocean and barrier layers, which will exert a vital influence on the processes of air-sea interaction and the regional climate around the SEAS (Nyadjro et al., 2012; Horii et al., 2016). Our findings demonstrate a potential role of BOB freshwater on short-term variability of monsoon over SEAS via interbasin water exchange.

Acknowledgements

We benefited from numerous datasets are freely available, including SMAP, GPCP, OAFlux, OSCAR, ASCAT, NOAA OLR, and HYCOM products.

References

Behara A, Vinayachandran P N, Shankar D. 2019. Influence of rainfall over eastern Arabian Sea on its salinity. Journal of Geophysical Research: Oceans, 124(7): 5003–5020, doi: 10.1029/2019JC014999

Da-Allada C Y, Gaillard F, Kolodziejczyk N. 2015. Mixed-layer salinity budget in the tropical Indian Ocean: seasonal cycle based only on observations. Ocean Dynamics, 65(6): 845–857, doi: 10.1007/s10236-015-0837-7

Feng Ming, Hacker P, Lukas R. 1998. Upper ocean heat and salt balances in response to a westerly wind burst in the western equatorial Pacific during TOGA COARE. Journal of Geophysical Research: Oceans, 103(C5): 10289–10311, doi: 10.1029/97JC03286

Gopalakrishna V V, Johnson Z, Salgaonkar G, et al. 2005. Observed variability of sea surface salinity and thermal inversions in the Lakshadweep Sea during contrast monsoons. Geophysical Research Letters, 32(18): L18605

Horii T, Ueki I, Ando K, et al. 2016. Impact of intraseasonal salinity variations on sea surface temperature in the eastern equatorial Indian Ocean. Journal of Oceanography, 72(2): 313–326, doi: 10.1007/s10872-015-0337-x

Huffman G J, Adler R F, Arkin P, et al. 1997. The Global Precipitation Climatology Project (GPCP) combined precipitation dataset. Bulletin of the American Meteorological Society, 78(1): 5–20, doi: 10.1175/1520-0477(1997)078<0005:TGPCPG>2.0.CO;2

Jayarathna W N D S, Du Yan, Zhang Yuhong, et al. 2018. Seasonal and interannual variability of sea surface salinity in the central north Arabian Sea based on satellite and Argo observations. Journal of Nanjing University of Information Science and Technology (Natural Science Edition), 10(3): 311–323

Kara A B, Rochford P A, Hurlburt H E. 2000. An optimal definition for ocean mixed layer depth. Journal of Geophysical Research: Oceans, 105(C7): 16803–16821, doi: 10.1029/2000JC900072

Li Yuanlong, Han Weiqing, Lee T. 2015. Intraseasonal sea surface salinity variability in the equatorial Indo-Pacific Ocean induced by Madden-Julian oscillations. Journal of Geophysical Research: Oceans, 120(3): 2233–2258, doi: 10.1002/2014JC010647

Li Xin, Yin Ming, Chen Xiong, et al. 2020. Impacts of the tropical Pacific–Indian Ocean associated mode on Madden–Julian oscillation over the maritime continent in boreal winter. Atmosphere, 11(10): 1049, doi: 10.3390/atmos11101049

Matthews A J, Singhruck P, Heywood K J. 2010. Ocean temperature and salinity components of the Madden–Julian oscillation observed by Argo floats. Climate Dynamics, 35(7–8): 1149–1168

Narvekar J, D'Mello J R, Prasanna Kumar S, et al. 2017. Winter-time variability of the eastern Arabian Sea: A comparison between 2003 and 2013. Geophysical Research Letters, 44(12): 6269–6277, doi: 10.1002/2017GL072965

Nyadjro E S, Subrahmanyam B, Murty V S N, et al. 2012. The role of salinity on the dynamics of the Arabian Sea mini warm pool. Journal of Geophysical Research: Oceans, 117(C9): C09002

Prakash S, Mahesh C, Mohan Gairola R. 2012. Observed relationship between surface freshwater flux and salinity in the north Indian Ocean. Atmospheric and Oceanic Science Letters, 5(3): 163–169, doi: 10.1080/16742834.2012.11446984

Price J F, Weller R A, Pinkel R. 1986. Diurnal cycling: Observations and models of the upper ocean response to diurnal heating, cooling, and wind mixing. Journal of Geophysical Research: Oceans, 91(C7): 8411–8427, doi: 10.1029/JC091iC07p08411

Rao R R, Sivakumar R. 2003. Seasonal variability of sea surface salinity and salt budget of the mixed layer of the north Indian Ocean. Journal of Geophysical Research: Oceans, 108(C1): 3009, doi: 10.1029/2001JC000907

Schiller A, Godfrey J S. 2003. Indian Ocean intraseasonal variability in an ocean general circulation model. Journal of Climate, 16(1): 21–39, doi: 10.1175/1520-0442(2003)016<0021:IOIVIA>2.0.CO;2

Schott F A, Xie Shangping, McCreary J P Jr. 2009. Indian Ocean circulation and climate variability. Reviews of Geophysics, 47(1): RG1002

Shankar D, Shetye S R. 1997. On the dynamics of the Lakshadweep high and low in the southeastern Arabian Sea. Journal of Geophysical Research: Oceans, 102(C6): 12551–12562, doi: 10.1029/97JC00465

Sun Qiwei, Du Yan, Zhang Yuhong, et al. 2019. Evolution of sea surface salinity anomalies in the southwestern tropical Indian Ocean during 2010–2011 influenced by a Negative IOD Event. Journal of Geophysical Research: Oceans, 124(5): 3428–3445, doi: 10.1029/2018JC014580

Vinayachandran P N, Kurian J, Neema C P. 2007. Indian Ocean response to anomalous conditions in 2006. Geophysical Research Letters, 34(15): L15602

Wang Lin, Kodera K, Chen Wen. 2012. Observed triggering of tropical convection by a cold surge: implications for MJO initiation. Quarterly Journal of the Royal Meteorological Society, 138(668): 1740–1750, doi: 10.1002/qj.1905

Wang Yanxin, Yang Xiaoyi, Hu Jianyu. 2016. Position variability of the Kuroshio Extension sea surface temperature front. Acta Oceanologica Sinica, 35(7): 30–35, doi: 10.1007/s13131-016-0909-7

Wu Yue, Liu Lin, Zheng Xiaotong. 2020. Influence of El Niño events on sea surface salinity over the central equatorial Indian Ocean. Environmental Research, 182: 109097, doi: 10.1016/j.envres.2019.109097

Wu Yue, Zheng Xiaotong, Sun Qiwei, et al. 2021. Decadal variability of the upper-ocean salinity in the Southeast Indian Ocean: Role of local ocean–atmosphere dynamics. Journal of Climate, 34(19): 7927–7942, doi: 10.1175/JCLI-D-21-0122.1

Xu Jindian, Gao Lu. 2018. The temporal-spatial features of evaporation and precipitation and the effect on sea surface salinity in the tropical Indian Ocean. Haiyang Xuebao (in Chinese), 40(7): 90–102

Zhang Yuhong, Du Yan. 2012. Seasonal variability of salinity budget and water exchange in the northern Indian Ocean from HYCOM assimilation. Chinese Journal of Oceanology and Limnology, 30(6): 1082–1092, doi: 10.1007/s00343-012-1284-7